Hydrodynamic development of a bionic pectoral fin for undersea monitoring platform

Yueri Cai, Xingwei Ren, Shusheng Bi, Guoyuan Li, Hans Petter Hildre & Houxiang Zhang

Published online: 21 Dec 2018.

Submit your article to this journal

Article views: 79

View related articles

View Crossmark data

Taylor & Francis
Taylor & Francis Group

Check for updates

Hydrodynamic development of a bionic pectoral fin for undersea monitoring platform

Yueri Cai [a], Xingwei Ren[a], Shusheng Bi[a], Guoyuan Li [b], Hans Petter Hildre[b] and Houxiang Zhang[b]

[a]Robotics Institute, Beihang University, Beijing, People's Republic of China; [b]Department of Ocean Operations and Civil Engineering, Norwegian University of Science and Technology, Ålesund, Norway

ABSTRACT

Bionic pectoral fins play an essential role in achieving the superior swimming ability of the bio-inspired undersea monitoring platform by producing desired movements and propulsion forces. This paper discusses the hydrodynamic modelling and experiments of a bionic pectoral fin inspired by the cownose ray. A simplified hydrodynamic model of the oscillatory bionic pectoral fin is built. A physical prototype of the bionic pectoral fin is developed based on the structure and movement parameters extracted from the cownose ray. Performances of the bionic pectoral fin in producing lift force and propulsion force are tested using a towing-tank experimental platform and compared with the results from corresponding simulations. Feasibility of the hydrodynamic simulation and the bionic design method are verified.

Nomenclature

|	
A	flapping amplitude
C_d	drag coefficient
C_y	chordwise length of pectoral section
f	flapping frequency
F_{y_aver}	average propulsion force
F_{z_aver}	average lift force
r	radius of transferred circle
U	velocity of incoming flow
y_l	y-coordinate of points on leading edge
y_t	y-coordinate of points on trailing edge
α	attack angle
β	pitch angle
θ	fin ray oscillatory angle
φ	fin ray oscillatory phase
Γ	circulation

1. Introduction

The offshore industry faces the challenge of bringing down operating and maintenance costs while meeting stringent safety requirements and the difficult of carrying out frequent maintenance and operations in the complex subsea environment (Pfeiffer et al. 2011; Chen et al. 2014). This presents challenges in terms of subsea operation, but also promotes technical innovations in the offshore industry (Kampmann et al. 2018). In order to provide detailed monitoring information of the offshore platform and the subsea installations efficiently and safely, the traditional offshore industry has undergone continuous technical innovation, especially in developing and employing the subsea operating mobile platform (Lee and Ku 2016; Mai et al. 2017; Mannam and Krishnankutty 2018; Sverdrup-Thygeson et al. 2018). Traditional subsea platforms propelled by screw propellers have some drawbacks when they are used in complex offshore environments, such as low efficiency when manoeuvring in limited space or a confined area with obstacles.

Fish can swim with high efficiency and high manoeuvrability, which provides an ideal model to solve the aforementioned problems (Bale et al. 2014; Asnafi 2016). Figure 1 shows a concept design of applying the bionic fish robot. It potentially has the ability to manoeuvre in confined space to help with efficient inspections. Fish have two kinds of swimming modes characterised by the body part that creates propulsion. They are the Body/Caudal Fin mode (BCF) and the Median and/or Paired Fin mode (MPF) (Webb 1984). Comparing with the fish using BCF mode, the fish using MPF mode possesses higher swimming stability and manoeuvrability (Blake 2004; Fish et al. 2017). The MPF mode can also be classified into two sub-modes, based on the number of transmission waves. One sub-mode is the oscillatory mode, in which one wave is transmitted on the pectoral fin of this sub-mode. The other one is the fluctuating mode, in which, more than one wave is transmitted on the pectoral fin. Comparing with the fish using fluctuating mode, the fish using oscillatory mode usually swims with higher velocity and higher efficiency (Rosenberger 2001; Fish et al. 2016).

The cownose ray is a typical fish utilising oscillatory mode movement. The oscillatory movement of its pectoral fin combines the chordwise pitching movement and the spanwise flapping movement. During the oscillatory movement, the motion phase of the leading edge is always ahead of the trailing edge. The special oscillatory movement of the pectoral fin contributes to the high performance swimming of the cownose ray. The undersea platform inspired by the cownose ray potentially has the features of high payload ability, high manoeuvrability and stability, rendering it suitable for undersea inspections and operation, such as high-quality visual inspection and the underwater thickness measurement, by carrying different kinds of sensors. Several bionic fish prototypes mimicking the cownose ray have been developed to explore its attracting
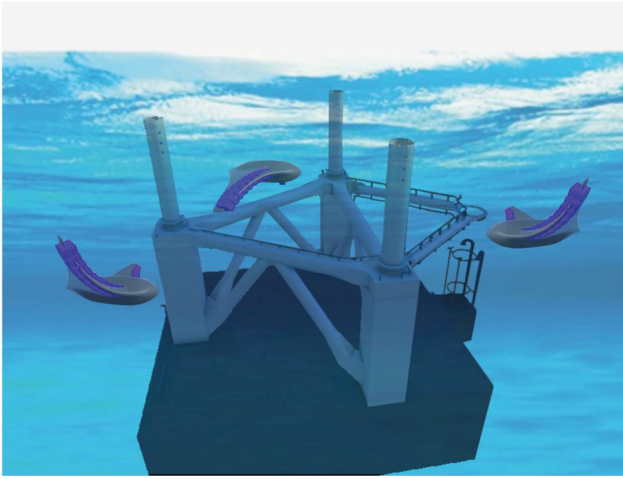
Figure 1. Concept design of the bionic fish robot inspired by the cownose ray, applied to survey the offshore platform (This figure is available in colour online).

Figure 2. The shape of the pectoral fin (This figure is available in colour online).

characteristics (Gao et al. 2009; Zhou and Low 2010; Elizabeth 2011; He and Zhang 2015; Li et al. 2016; Imahama et al. 2018). The explorations mostly focus on realising the self-propelled swim. Most of them have adopted a kind of simplified structure and layout for a feasible design. However, the swimming performance, including the velocity, stability, manoeuvrability and duration, are far inferior to the real cownose ray. Therefore, the hydrodynamic mechanism of the oscillatory movement requires further analysis and experimental verification.

This paper illustrates development and verification of a bionic pectoral fin with multiple fin rays. The pectoral fin can realise the oscillatory movement mimicking the cownose ray, with both actively controllable deformation and passive flexible deformation. It plays an important role as the main propulsion part of the future bionic undersea platform inspired by the cownose ray. The simplified hydrodynamic simulation model of the pectoral fin is constructed, based on the blade-element theory. Then, the hydrodynamic performances of the designed bionic pectoral fin are simulated. A towing-tank experimental platform is built to test the lift force and propulsion force produced by the bionic pectoral fin. The testing results are compared with the simulation results to verify the feasibility of the simulation method, and the design feasibility of the bionic pectoral fin.

2. Materials and methods

2.1. Shape and movement of the pectoral fin

The plane shape of the cownose ray can be simplified to a triangle-like shape. As shown in Figure 2, the bionic pectoral fin with fin base length of 0.36 m and a span length of 0.3 m is utilised in this paper. The curve of the leading edge of the pectoral fin is simplified to a linear curve.

$$y_l(x) = -0.5x. \tag{1}$$

The trailing edge curve is a little more complicated, which can be simplified and fitted by a quadratic curve.

$$y_t(x) = -0.002x^2 + x - 360. \tag{2}$$
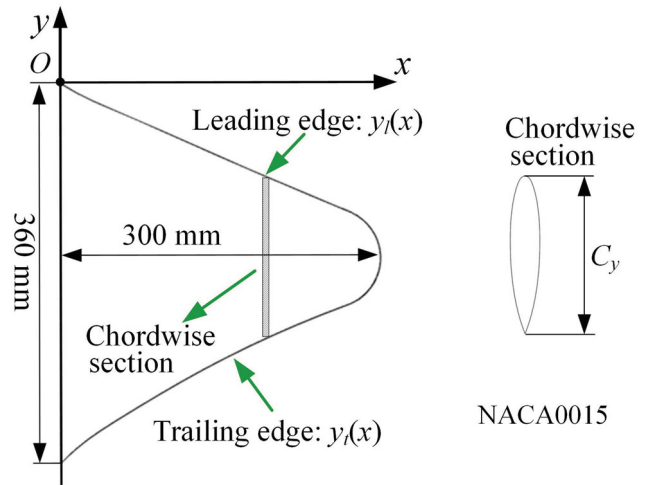
The tip part of the pectoral fin is fitting with an arc curve to make the pectoral fin sideline smooth. The chordwise sections of the pectoral fin of the cownose ray can be simplified to a series of NACA shape airfoils (Heine 1992). Here, we apply the NACA0015 shape airfoils uniformly along the spanwise direction.

Based on our observations of the cownose ray in the aquarium and the biological research (Russo et al. 2015; Fish et al. 2017), its movement has several: (1) the complicated oscillatory movement of the pectoral fin consists of two sub-movements, the spanwise flapping movement and the chordwise pitching movement; (2) a simplified understanding of the deformation of each spanwise section can be extracted as a time-related cubic curve (Cai et al. 2012); (3) oscillating frequency of the pectoral fin is low, usually lower than 1 Hz, according to video-based analysis of the free swimming cownose ray; (4) the flapping amplitude of the pectoral fin tip is as large as half of the fin base length; and (5) 0.2–0.5 full transmission waves pass on the pectoral fin is around. The movement of the bionic prototype is simplified to periodic flapping movement of three fin rays. As shown in Figure 3,
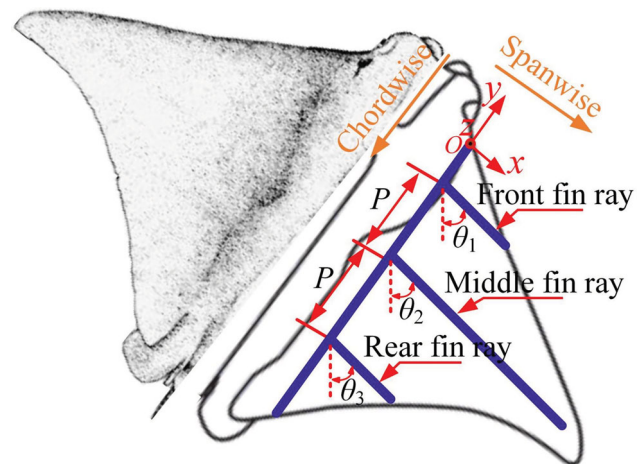
Figure 3. Simplified schematic of the pectoral fin (This figure is available in colour online).

the fin rays are placed along the chordwise direction with uniform intervals. The length of the interval is P. The fin ray placed in the middle plays an essential role of realising the flapping movement about the y-axis. The fin rays placed at the front and at the rear play a role in obtaining the pitching movement. At the same time, the two fin rays assist the middle fin ray in the flapping movement. The wave transmitted on the pectoral fin is performed by the pitching movement.

Then, the movement discipline applied to the fin rays is:

$$\theta_i = A_i \sin\left(2\pi f_i t + \varphi_i\right) \quad i = 1, \quad 2, \quad 3, \tag{3}$$

where θ_i represents the oscillatory angle according to the y-axis of each fin ray, A_i represents the flapping amplitude of each fin ray, φ_i represents the phase difference between two adjacent fin rays, and f_i is the oscillatory frequency of the pectoral fin and is applied to each fin ray identically. As mentioned before, the oscillatory movement of the pectoral fin consists of the two sub-movements, the flapping movement about y-axis and the pitching movement about x-axis. The phase differences between the two neighbouring fin rays are controlled to be equal.

2.2. Hydrodynamic analysis of the pectoral fin

According to the simplification of the leading edge and the trailing edge of the pectoral fin, the length of each chordwise section is:

$$C_y = y_l - y_t. \tag{4}$$

The force condition of the chordwise section is shown in Figure 4. In it, v_y is the swimming velocity or towing velocity applied to the pectoral fin, v_r is the induced velocity generated by the oscillatory pectoral fin, β is the pitching angle that is controlled by the phase difference between each pair of neighbouring fin rays, and α is the attack angle. Then, α can be calculated.

$$\alpha = \arctan\left(v_r/v_y\right) - \beta, \quad v_y \neq 0. \tag{5}$$

Based on the Kutta–Joukowski theorem (Dong 2003), the circulation around the chord section in the condition of the plane potential flow can be calculated as:
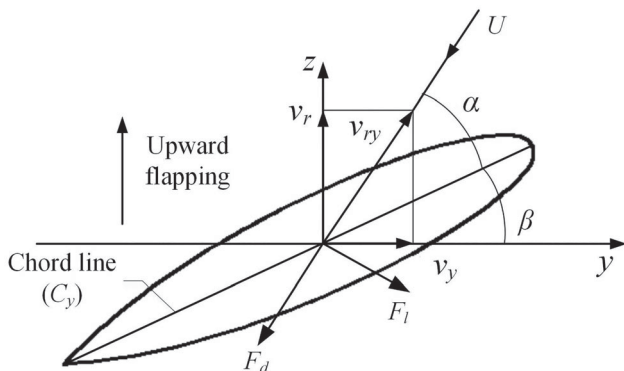
$$\Gamma = 4\pi U r \sin\alpha, \tag{6}$$

where U is the velocity of the incoming flow and r is the radius of the transferred circle.

Then, the lift force generated by the chord section can be derived by:

$$dF_l = \rho U \Gamma d_r. \tag{7}$$

The drag force applied on the chord section is:

$$dF_d = C_d \rho U^2 C_y d_r / 2, \tag{8}$$

where ρ is the density of water, C_d is the standard drag coefficient of NACA0015 shape airfoil, the value of C_d is related with the attack angle α:

$$C_d = 0.00119\alpha^2 - 0.056\alpha + 0.04. \tag{9}$$

The propulsion force and the lift force generated by the chordwise section is:

$$\begin{cases} dF_y = dF_l \sin\left(\alpha + \beta\right) - dF_d \cos\left(\alpha + \beta\right) \\ dF_z = \left(dF_l \cos\left(\alpha + \beta\right) + dF_d \sin\left(\alpha + \beta\right)\right) \cdot \cos\theta \end{cases} \tag{10}$$

The average propulsion force and the average lift force are:

$$\begin{cases} F_{y\_aver} = \dfrac{1}{T} \int_0^T F_y(t)dt, \\ F_{z\_aver} = \dfrac{1}{T} \int_0^T F_z(t)dt. \end{cases} \tag{11}$$

2.3. Modelling simulation of the pectoral fin

A simulation is carried out according to the above theoretical analysis. The simulation programme has the required functions, including that (a) building the bionic pectoral fin model automatically with the input structure parameters. The parameters of the bionic pectoral fin are expressed by the Equation (1), Equation (2) and Figure 2; (b) setting the movement parameters of the bionic pectoral fin, including the flapping frequency, flapping amplitude, phase difference and swimming speed; (c) calculating the lift force and propulsion force automatically, according to the theoretical analysis; (d) presenting the simultaneous lift force and propulsion force, and their average values. The processing flow of the simulation is shown in Figure 5.

In the simulation, the fin rays can have different flapping amplitude, but with the same flapping frequencies, in order to keep the required spatial movement deformation of the bionic pectoral fin. The movement phase of the front fin ray is set as the basement and the phase differences of the middle fin ray and the rear fin ray are decided accordingly. The incoming flow velocity is used to simulate the swimming speed of the bionic pectoral fin. The preset movement parameters in the simulation are summarised in Table 1.

Figure 6 shows the instantaneous lift force and instantaneous propulsion force of the designed bionic pectoral fin, which are simulated under the following movement parameters: (1) the distance between the adjacent fin rays is $P = 90$ mm; (2) the flapping amplitude of each fin ray is $A_i = 15°$; (3) the flapping frequency of each fin ray is $f = 0.4$ Hz; (4) the incoming flow velocity, that is, the swimming speed of the bionic pectoral fin is $v = 0.3$ m/s. It can be ascertained that both the
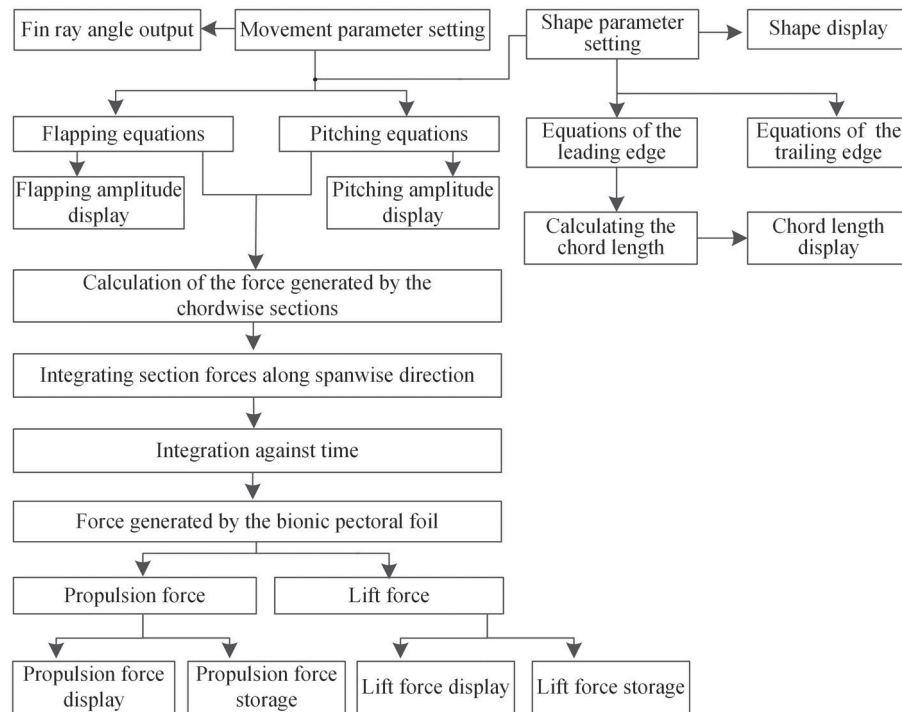

Figure 4. Forces on the chordwise section.

Figure 5. Processing flow of the simulation.

lift force and the propulsion force vary according to sinusoidal rule. The average lift force in a movement cycle is zero. Therefore, the pitch motion will appear during the cownose ray swims. At the middle position, the bionic pectoral fin produces the maximum lift force and propulsion force. The minimum values are obtained at the amplitude position. This is caused by changes of the effective attack angles, meaning that the maximum effective attack angle appears at the middle position.

2.4. Bionic pectoral fin development and experimental setup

The inside skeleton of the bionic pectoral fin is made of three specially designed fin rays. The shape of each is decided according to the deformation requirements of the oscillatory pectoral fin. Figure 7(a) shows the dimension sketch of the middle fin ray, which plays the most important role in producing the main propulsion force. Figure 7(b) provides the deformation verification of the middle fin ray, by comparing the results of the simulation and load test. The simulation is carried out using ANSYS. Rigidity and elasticity of the fin ray are optimised by arranging the dimensions, according to the multiple simulations and load tests, to make the fin ray bend to fit the curve that we observed and simplified from the cownose ray (Cai et al. 2012). Deformation curves of the middle fin ray under the static load applied at the fin tip fit with the simulated

curve well, which can partly verify its bionic deformation ability. Figure 7(c) shows the specific dimensions of the middle fin ray skeleton. The front fin ray and the rear fin ray are designed in the same way. All the three fin rays are made of carbon fibre plate.

The development process of the bionic pectoral fin prototype is shown in Figure 8. In Figure 8(a), each fin ray is driven by an independent gear motor. Therefore, the flapping amplitude, the flapping frequency, and the movement phase of each fin ray can be controlled independently. In order to make the inside fin rays and the soft body bond firmly, and make the movement deformation between the fin rays smooth, elastic connections are placed at regular intervals between the fin rays, as shown in Figure 8(b). A mold in Figure 8(c) is designed based on the simplified shape of the soft body. Two sub-molds are used to make the demoulding easier. The soft body of the pectoral fin is poured by a customised RTV-2 liquid silicone rubber (Chen et al. 2010). After solidification, the
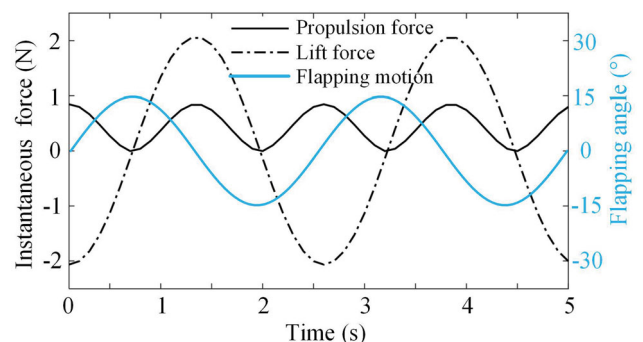
Table 1. Movement parameter settings.

Parm	Declaration	Unit	PARM	Declaration	Unit
A1	Front fin ray amplitude	deg.	φ_1	Front fin ray phase	deg.
A2	Middle fin ray amplitude	deg.	φ_2	Middle fin ray phase	deg.
A3	Rear fin ray amplitude	deg.	φ_3	Rear fin ray phase	deg.
f	Flapping frequency	Hz	U	Incoming flow velocity	m/s

Figure 6. Simulated instantaneous propulsion force and lift force (This figure is available in colour online).
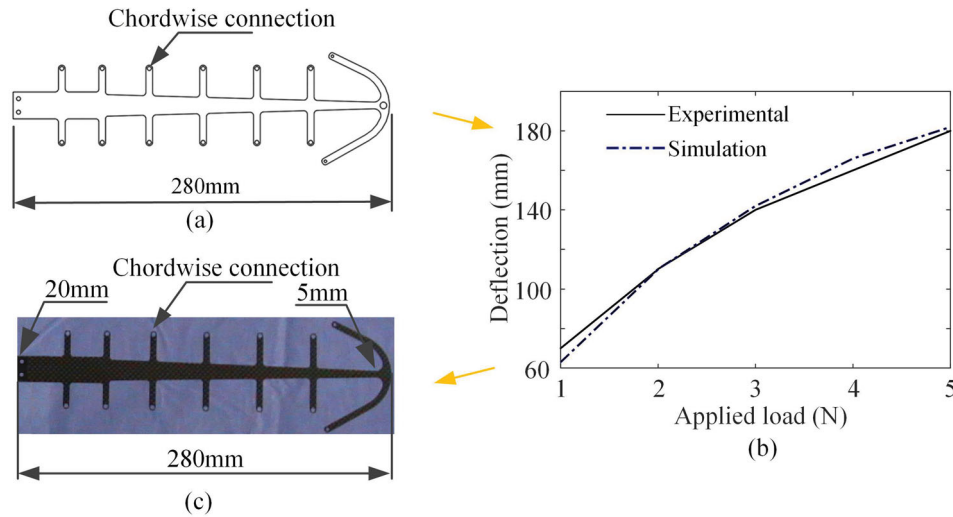
Figure 7. Design and optimization of the middle fin ray consisting of. (a) schematic design; (b) simulation and experimental tests of the deflection; and (c) main structural parameters (This figure is available in colour online).

hardness of the soft body is Shore 20°. The elasticity of the silicone rubber after curing can reach twice its original length. The outer shape of the bionic pectoral fin is formed by the designed mold. The shape of each chordwise section is formed to the NACA0015 shape. The roughness of the soft body skin is mainly decided by the inner surface of the mold, which is polished by sanding with the final roughness of around Ra3.2. The developed soft bionic pectoral fin for testing is shown in Figure 8(d). The movement parameters that can be achieved by the bionic pectoral fin is summarised in Table 2.

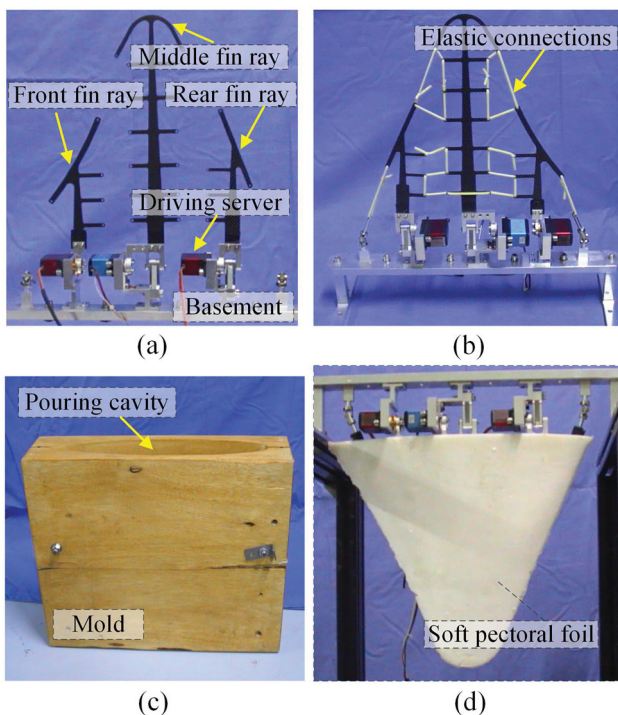The testing unit with force sensors is connected with the basement of the bionic pectoral fin. The bionic pectoral fin is placed vertically in the water. Two S-shape HSTL-BLSM force sensors are used to measure the propulsion force and lift force generated by the pectoral fin prototype. The range of the force sensor is 0–20 N, and measuring accuracy is 0.03% FS. The force sensors have been calibrated by suspension test with standard weights. The parameters of the towing experimental platform are summarised in Table 3. The propulsion force and lift force measured are corrected by the calibration results in the experiments. As shown in Figure 9, the testing unit is mounted on the towing platform. The towing platform can move with a maximum velocity of 0.5 m/s. The free swimming of the bionic fish robot is performed by the towing movement. Propulsion force and lift force produced by the bionic pectoral fin are measured by the force sensors directly. The force signals are collected by the NI DAQ6008 data acquisition card. The acquisition frequency is set to 100 Hz. A low pass filter is applied to eliminate the signal noises.

3. Results and discussion

Figure 10 shows the movement deformation of the bionic pectoral fin prototype. The spanwise deformation curve of the trailing edge at a time point is recorded and fitted by nine markers, as shown in Figure 10(a). The curve fits the spanwise movement deformation rule of the cownose ray's pectoral fin. That is, it performs a deformation rule consistent with the cubic equation observed. Figure 10(b) shows the driving wave transmitted along the chordwise direction. The designed phase differences between the fin rays are achieved. The movement phase of the marker on the middle of the leading edge is advanced ahead of the marker on the middle point of the trailing edge.

Figure 8. Development of the pectoral fin prototype including (a) the inside fin rays with driving servers; (b) the inside skeleton with elastic connections; (c) the mold; and (d) the prototype (This figure is available in colour online).

Table 2. Parameters of the bionic pectoral fin.

Variables	Symbol	Unit	Value range
Flapping amplitude	A_{max}	deg.	0–25
Oscillatory frequency	f	Hz	0.1–0.6
Phase difference	φ	deg.	0–60
Towing velocity	v_y	m/s	0–0.5

Table 3. Parameters of the sensors and the experimental platform.

Towing speed range	0–0.5 m/s
Number of force sensor	2
Sensor force range	0–20 N
Measuring accuracy	0.03%F S
Output signal	4–20 mA or +/−10 V

The instantaneous lift force and propulsion force produced by the bionic pectoral fin prototype are shown in Figure 11(a) and (b), respectively. The movement parameters are set as follows: the towing velocity is 0.2 m/s, the oscillatory frequency is 0.4 Hz, the oscillatory amplitude is 18° and the phase difference between each pair of fin rays is 25°. The instantaneous propulsion force varies periodically as obtained from the simulation. The frequency of the propulsion force is twice of the oscillatory frequency, which is caused by the fact that the bionic pectoral fin can generate propulsion force both in the upward and in the downward flapping movements. The maximum lift force produced by the pectoral fin prototype reaches near 1 N. The maximum propulsion force can occasionally go beyond 0.5 N. Self-propulsion ability is performed by the prototype, attributing to the positive average propulsion force obtained. Compared with the simulation results, the lift force and the propulsion force are in consistent with the same changing rule.

The structure parameters and the movement parameters influence the forces generated by the bionic pectoral fin generates. For the specific flapping pectoral fin developed, the propulsion force can be taken as a sub-force of the produced lift force. The structure parameters are decided by the bionic design based on observations of the cownose ray. The movement parameters that can be controlled actively play an important role in generating swimming forces. Influences of the oscillatory amplitude, the oscillatory frequency and the phase difference are simulated and tested via prototype. The movement parameters are set as shown in Table 4. Within the testing ranges of the parameters, the feasibility of the simulation is verified by experiments qualitatively.

Figure 12(a) shows the influence of the oscillatory amplitude on producing the propulsion force. Within the testing range of

Figure 10. Movement deformation of the bionic pectoral fin. (a) spanwise trailing edge deformation; (b) chordwise deformation along the edges. MPoT, FT and MPoL are abbreviations of the middle point on the trailing edge, the fin tip and the middle point on leading edge, respectively (This figure is available in colour online).

the amplitude from 2° to 22°, the propulsion force increases with the oscillatory amplitude. The simulation results show an identical changing rule as the experiments. The highest average propulsion force is 0.6 N, when the oscillatory amplitude is 22°. The maximum error between the simulation results and the experimental results is 0.12 N, which is obtained at the oscillatory amplitude of 22°.

Figure 12(b) shows the influence of the oscillatory frequency on producing the propulsion force. The frequencies change from 0.1 to 0.5 Hz, which the cownose ray typically uses in straight forward swimming. Within the frequency range, the propulsion force increases with the oscillatory frequency. As the frequency increases, the experimental propulsion force produced by the bionic pectoral fin gradually becomes smaller than that of the simulation. The maximum difference value is 0.18 N, which is obtained at the oscillatory frequency of 0.5 Hz.

Figure 12(c) shows the influence of the phase difference on producing the propulsion force. Typically, there are 0.2–0.5 waves transmitting along the chordwise direction of a cownose ray's pectoral fin when it swims forward straightly. These wave

Figure 9. The experimental setup (This figure is available in colour online).
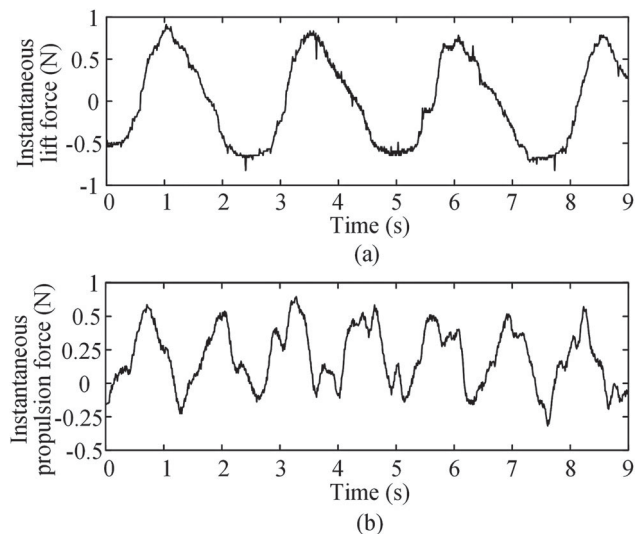
Figure 11. Experimental lift force and propulsion force. (a) the lift force; (b) the propulsion force.

Table 4. Parameters utilised in the experiments.

Variables	Unit	Amplitude	Frequency	Phase difference	Towing speed
Oscillatory amplitude	deg.	**2–22**	20	12	15
Oscillatory frequency	Hz	0.4	**0.1–0.5**	0.3	0.4
Phase difference	deg.	25	30	**10–60**	35
Towing speed	m/s	0.2	0.3	0.2	**0–0.4**

numbers are equal to the phase difference of 18° to 45° between two adjacent fin rays. In the experiments, the phase differences are changed from 10° to 60°. Within the testing range, the propulsion force increases at first and then decreases with the phase difference. The maximum propulsion force that appears around the phase difference is about 20°. The difference values between the simulated results and the experimental results vibrate within 0.1 N. The decreasing changes partly caused by the specific NACA0015 shape chordwise sections.

Figure 12(d) shows the influence of the towing speed on producing the propulsion force. The towing motion is used to mimic the free swimming condition of the fish robot. In the test range, the towing speed varies from 0 to 0.4 m/s which is equal to the swimming speed of 0–0.7 BL/s of the further developed fish robot using the bionic pectoral fin proposed here. In this range, the average propulsion force decreases as the towing speed increases. The errors between the simulated results and the experimental results are less than 0.2 N.

Another force that directly affects the swimming performance of the bionic fish robot is the lift force. The fish robot needs a slightly positive lift force to keep and adjust the swimming depth. On the other hand, the maximum value of the lift

force affects the pitch motion of the fish robot, which is the main swimming ability performance.

Figure 13(a)–(d) shows how the changing of the movement parameters affects the maximum lift force. The parameters used are the same as those used in average propulsion force tests. Figure 13(a) shows the influence of the oscillatory amplitude on producing the maximum lift force. The maximum lift force increases with the oscillatory amplitude, which means that the pitch motion amplitude becomes larger in equal law. It makes the swimming ability poorer. The differences between the experimental results and the simulation results vary within 0.5 N of this range of flapping amplitudes.
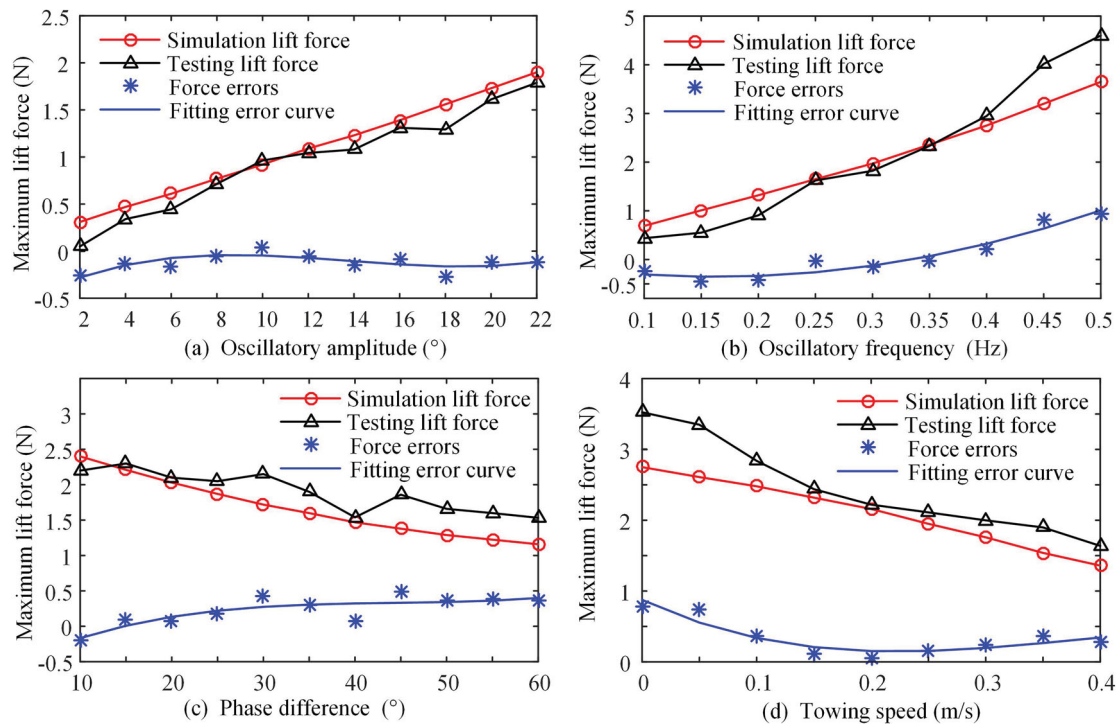
The influence of the oscillatory frequency shown in Figure 13(b) illustrates a similar law as the oscillatory amplitude performs. Referring to the propulsion force experiments, increasing the oscillatory amplitude and the flapping frequency both benefit by producing the propulsion force, which means it is good for obtaining higher swimming velocity. But, the higher the oscillatory amplitude and the oscillatory frequency, the poorer the swimming stability performance. In the oscillatory frequency tests, the value difference between the simulation results and the experimental results can reach near 1 N, which is under the flapping frequency of 0.5 Hz.

Figure 13(c) shows the influence of changing the phase difference from 10° to 60°. The maximum lift force gradually decreases. The difference values between the simulation and the experimental results fluctuate within plus/minus 0.5 N. Changing the towing speed makes the maximum lift force change with same rule as changing the phase difference. The results are shown in Figure 13(d). This means that the bionic pectoral fin prototype performs better swimming
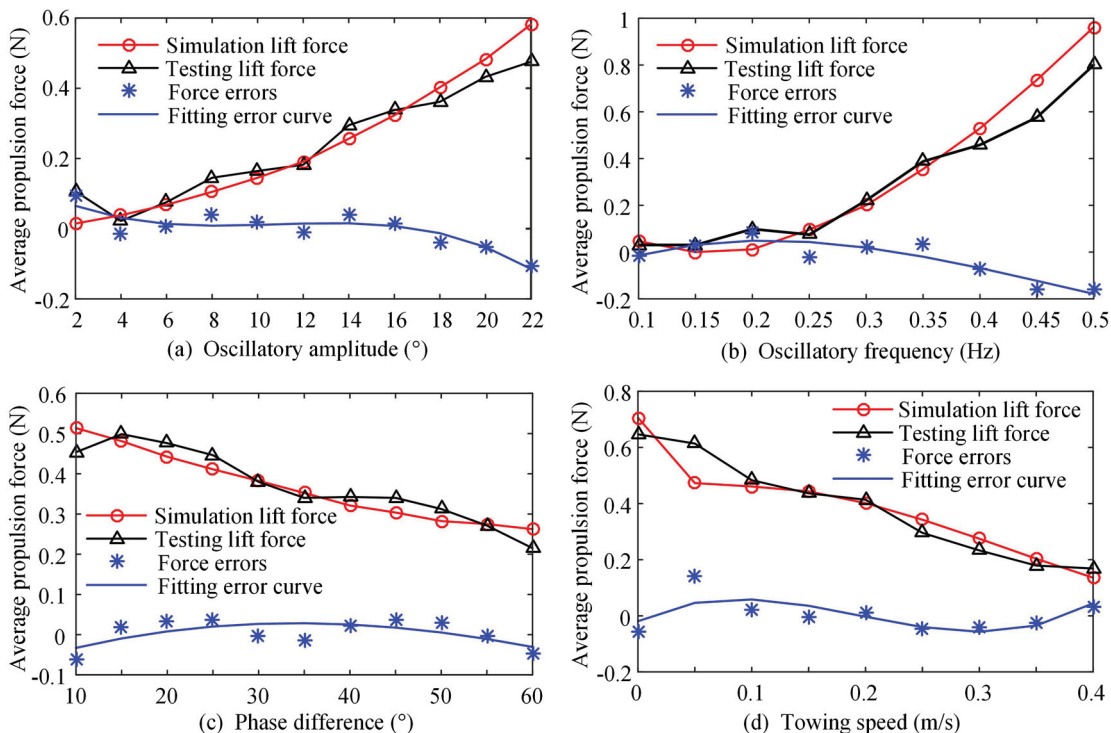
Figure 12. Influence of the movement parameters on the average propulsion force, including (a) the oscillatory amplitude; (b) the oscillatory frequency; (c) the phase difference; and (d) the towing speed (This figure is available in colour online).

Figure 13. Influence of the movement parameters on the maximum lift force, including (a) the oscillatory amplitude; (b) the oscillatory frequency; (c) the phase difference; and (d) the towing speed (This figure is available in colour online).

stability with lower values of phase difference and swimming velocity.

4. Conclusions

The fish robot inspired by the cownose ray provides a novel solution for developing an underwater platform to fulfil the requirements of subsea inspection and other complex operations. The bionic pectoral fin is the most important part to realise the biomimetic propulsion. With the well using the bionic oscillatory pectoral fin, the undersea platform can potentially obtain high efficiency and highly manoeuvrable movement. Therefore, the bionic pectoral fin has been designed, simulated and tested experimentally in this paper. The structure parameters and movement discipline obtained from the cownose ray are simplified to direct the bionic design. A simulation model based on the blade-element theory has been built to analyse the performance of the bionic pectoral fin. The simulation is carried out according to the theoretical analysis. A bionic pectoral fin prototype is developed accordingly. It is driven by three independent fin rays. The basic movement rule of the cownose ray is achieved by the prototype. Within the testing ranges, the simulation method is verified by the experiments to some extent, but the simulation presented is simplified based on the blade-element theory. It provides the qualitative results that illustrate the same change tendency, compared with the computational fluid dynamics analysis. There are still visible errors between the simulation results and the experimental results.

The feasibility of the simulation method and the development method of the bionic pectoral fin aiming to supply a bionic underwater propulsion solution has been verified. The simulation method and the design process of the bionic pectoral fin illustrated in this paper provides a reference for developing the kind of bionic underwater platform.

ORCID

Yueri Cai 🔟 http://orcid.org/0000-0003-4494-6300
Guoyuan Li 🔟 http://orcid.org/0000-0001-7553-0899

References

Asnafi A. 2016. A method to investigate general optimal maneuvers for kinematically reducible robotic locomotion systems. J Intel Robot Syst. 84(1–4), 799–813.

Blake RW. 2004. Fish functional design and swimming performance. J Fish Biol. 65(5): 1193–1222.

Bale R, Hao M, Bhalla APS, Patankar NA. 2014. Energy efficiency and allometry of movement of swimming and flying animals. Proc Natl Acad Sci USA. 111(21), 7517–7521.

Cai Y, Bi S, Zheng L. 2012. Design optimization of a bionic fish with multi-joint fin rays. Adv Robot. 26(1–2), 177–196.

Chen D, Yi S, Wu W, Zhong Y, Liao J, Huang C, Shi W. 2010. Synthesis and characterization of novel room temperature vulcanized (RTV)

silicone rubbers using vinyl-POSS derivatives as cross linking agents. Polymer. 51(17):3867–3878.

Chen H, Stavinoha S, Walker M, Zhang B, Fuhlbrigge T. 2014. Opportunities and challenges of robotics and automation in offshore oil & gas industry. Intell Control Autom. 5(03): 136.

Dong C. 2003. Nonviscous fluid mechanics. Bejing: Tsinghua University Press. 253–259.

Elizabeth P. 2011. Bio-inspired engineering: manta machines. Science. 232: 1028–1029.

Fish FE, Schreiber CM, Moored KW, Liu G, Dong H, Bart-Smith H. 2016. Hydrodynamic performance of aquatic flapping: efficiency of underwater flight in the manta. Aerospace. 3(3): 20.

Fish FE, Dong H, Zhu J, Bart-Smith H. 2017. Kinematics and hydrodynamics of mobuliform swimming: oscillatory winged propulsion by large pelagic batoids. Mar Technol Soc J. 51(5), 35–47.

Gao J, Bi S, Li J, Liu C. 2009. Design and experiments of robot fish propelled by pectoral fins. IEEE International Conference on Robotics and Biomimetics (ROBIO), 19–23. December, Guilin, Guangxi, China, pp. 445–450. doi:10.1109/ROBIO.2009.5420688.

Mai C, Pedersen S, Hansen L, Jepsen K, Yang Z. 2017. Modeling and control of industrial ROV's for semi-autonomous subsea maintenance services. IFAC-PapersOnLine. 50(1): 13686–13691.

Heine CE. 1992. Mechanics of flapping fin locomotion in the cownose ray, *Rhinoptera bonasus* (Elasmobranchii: Myliobatidae), PhD Dissertation, Duke University, USA.

He J, Zhang Y. 2015. Development and motion testing of a robotic ray. J Robot. 2015: 791–865.

Imahama T, Watanabe K, Mikuriya K, Nagai I. 2018. A method for calculating the amount of movements to estimate the self-position of manta robots. J Phys Conf Ser. 962(1): 012–016.

Kampmann P, Christensen L, Fritsche M, Gaudig C, Hanff H, Hildebrandt M, Kirchner F. 2018. How AI and robotics can support marine mining. Offshore Technology Conference. 30 April-3 May, Houston, Texas, USA, OTC-29069-MS.

Lee D, Ku NK. 2016. Robotic orthosis to assist overhead operations for double hull structure. Ships Offsh Struct. 11(8): 880–889.

Li G, Deng Y, Osen OL, Bi S, Zhang H. 2016. A bio-inspired swimming robot for marine aquaculture applications: from concept-design to simulation. OCEANS, 10–13. April, Shanghai, China, pp. 1–7. doi:10.1109/OCEANSAP.2016.7485691.

Mannam NPB, Krishnankutty P. 2018. Hydrodynamic study of flapping foil propulsion system fitted to surface and underwater vehicles. Ships Offsh Struct. 13(6): 575–583.

Pfeiffer K., Bengel M, Bubeck A. 2011. Offshore robotics-survey, implementation, outlook. IEEE/RSJ International Conference on Intelligent Robots and Systems (IROS), 25-30, September, San Francisco, California, USA, pp. 241–246.

Rosenberger LJ. 2001. Pectoral fin locomotion in batoid fishes: undulation versus oscillation. J Exp Biol. 204(2): 379–394.

Russo RS, Blemker SS, Fish FE, Bart-Smith H. 2015. Biomechanical model of batoid (skates and rays) pectoral fins predicts the influence of skeletal structure on fin kinematics: implications for bio-inspired design. Bioinspir Biomim. 10(4): 046002.

Sverdrup-Thygeson J, Kelasidi E, Pettersen KY, Gravdahl JT. 2018. The underwater swimming manipulator – a bioinspired solution for subsea operations. IEEE J Oceanic Eng. 43(2), 402–417.

Webb PW. 1984. Form and function in fish swimming. Sci Am. 251(1): 72–83.

Zhou C, Low KH. 2010. Better endurance and load capacity: an improved design of manta ray robot (RoMan-II). J Bionic Eng. 7(4): S137–S144.